Combustion model for thermite materials integrating explicit and coupled treatment of condensed and gas phase kinetics

Emelian Tichtchenko, V. Folliet, Olivier Simonin, Benoît Bédat, L. Glavier, Alain Estève, Carole Rossi

Combustion model for thermite materials integrating explicit and coupled treatment of condensed and gas phase kinetics

E. Tichtchenko[a,c], V. Folliet[a], O. Simonin[b], B. Bédat[b],
L. Glavier[c], A. Esteve[a], C. Rossi[a,*],

[a] *LAAS-CNRS, University of Toulouse, 7 Avenue du Colonel Roche, 31400 Toulouse*
[b] *Institut de Mécanique des Fluides de Toulouse (IMFT), Université de Toulouse, CNRS, France*
[c] *ArianeGroup, 66 Route de Verneuil, 78130 Les Mureaux*

01/05/2021

Abstract

Nanothermites are interesting energetic systems as their combustion driven by the oxidation of the metallic fuel associated with the reduction of the oxidizer, can produce extremely fast burning rates exceeding hundreds of $m.s^{-1}$. In addition, by changing the reactant (composition, stoichiometry) geometry and compaction conditions, the control of the burning rate can be achieved, allowing the designer to customize the chemical energy for each application. To date, only rough combustion models exist, most restricting the combustion mechanisms to only condensed phase processes, thus providing an approximative prediction of structure-combustion performance relationships. This work presents a tri-phasic model for the combustion of Al/CuO powder considering 9 gaseous species (Al, Cu, O_2, O, Al_2O, Al_2O_2, AlO, AlO_2, N_2) and 4 condensed species (Al, Cu, CuO, Al_2O_3) that can be liquid or solid. The reactionnal scheme involves 12 heterogeneous reactions and 2 phase changes based on diffusional kinetics, while gaseous reactions are considered through a chemical equilibrium. A detailed description of the theoretical formulation and numerical method is presented, followed by a discussion of a closed-bomb simulation. This work highlights the great impact of the Al particles initial diameter on the pressure development in the chamber. After the initiation stage, the decomposition of CuO releases gaseous O_2, which is spontaneously absorbed on the surface of submicronic Al particles and diffuses through alumina to react with pure Al. At high temperature, gaseous copper, aluminum sub-oxides and aluminum condense on both particle types. By contrast, Al particle micron-size limits the quantity of O_2 absorption and gaseous species surface condensation, leading to the formation of a pressure pre-peak 4 times higher than the final chamber pressure.

Keywords: Combustion, Al/CuO, nanothermite, numerical simulation, multiphase

1. Introduction

Thermites are composed of nano-micro sized metals (Al, Mg, Ti, B) and metal oxides (CuO, Fe_2O_3, Bi_2O_3, MoO_3 ...), which both participate in a highly exothermic and self-propagating combustion reaction accompanied with gas release in most cases. Interestingly, the reactant (oxide, fuel) geometry, composition and compaction conditions can be varied to tune their combustion characteristics making these materials of major interest for a number of applications, such as soldering/welding, generation of biocidal-agents and as additives in propellants, pyrotechnics and explosives. This combustion behavior variability imposes to rationalize experiments, guided by suitable modeling approaches. Several continuum/analytical models have been proposed to capture the reactants size, stoichiometry and porosity effects during nanothermite powder combustion. Kim *et al.* [1] developed a simplified modeling analysis based on a 1D continuum heat transfer model using an activation energy associated with Al oxidation reaction to appreciate the ignition and combustion propagation characteristics in the Al/MoO_3 nanoscale thermite. Along the same line, Brotman *et al.* [2] proposed a 1D modelling scheme integrating further mechanisms being characteristics of thermites reaction, such as the thermally activated transports of oxygen atoms, in association with the multiple barrier layers, fuel and oxidizer phase transformation. In all these approaches, the mass transport rate driving the reaction, described by exponential Arrhenius law [3, 4], is coupled with the heat transfer in order to compute the initiation and combustion characteristics. However, they restrict the reaction mechanisms to condensed phase processes only. Interestingly, Epps *et al.* [5] introduced a non-dimensional continuum modelling approach accounting for the first time the advection of gas contained in the porous thermite matrix via a Darcy's law. The objective of this work being to enable a parametric investigation of the important physical characteristics during the Al/CuO nanothermite combustion (conductive *vs* advective combustion regimes), the global chemistry of the thermite reaction is reduced to a single Arrhenius law with a rough estimate of the gas released. Another approach developed by Baijot *et al.* [6] to study pressurization of manometric bombs integrates an set of physicochemical mechanisms, both in the condensed and gas phases, including diffusion of species, decomposition of materials, vaporization/condensation at interfaces, and gas phase reactions. No heat exchange was considered between gas and condensed phases, nor between fuel and oxidizer particles. Despite this simplification, reasonably good agreement between predicted and measured pressure development was obtained, but in a limited pressure range and for very particular experimental conditions. The purpose of the present study is to implement into the Baijot's model new physical mechanisms derived from recent advances in the fundamental understanding of Al/CuO nanothermite combustion [7–12].

For that purpose, a tri-phasic system (fuel, oxide and gas phases) is considered to explore the ignition and combustion of thermite powders. We computed a set of physicochemical processes in the condensed and in the gas phases. The model is applied to an Al/CuO system as it is the most documented. The system is composed of three phases: two particle phases and one gaseous noted p, q, and g respectively. Condensed species inside a particle phase (Al, Al_2O_3, CuO, Cu) can be liquid or solid, and phase change is considered from an energetic point of view. Condensed species are assumed immiscible and their densities constant. The particles inside a particle phase $k = p, g$ are assumed spherical during the whole simulated time, characterized by an inner and outer diameter respectively d_k^{in} and d_k : the difference between both defines the alumina shell thickness. Particles $k = p, q$ are assumed isothermal and no mass exchange between the two particle phases is considered.

The gas phase involves 9 species (Al, Cu, O_2, N_2, Al_2O, Al_2O_2, AlO, AlO_2, O). Homogeneous reactions rates assumed fast, gas is treated at equilibrium and an explicit description of heterogeneous reactions is proposed based on diffusional kinetics. After the description of the theoretical formulation and numerical method, the combustion principles at constant volume is discussed at the light of structural features as well as the physico-chemical parameters which are shown to govern the combustion dynamics in Al/CuO thermite systems.

2. Physical model and conditions

The three phases, noted p, q and g, represent the aluminum particle phase, the copper particle phase, and the gas phase, respectively. The main heterogeneous reactions and phase transitions involved between the condensed (p, q) and the gas (g) phases are (cf. Table 1 for the set of chemical reactions) :

- Oxydation of aluminum in the p core by O_x species (O_2 and O) through reactions R1, R2.
- decomposition of CuO releasing oxygen species in the gas through reaction R5.
- decomposition of the alumina shell, which generates molecular oxygen and atomic aluminum through reaction R3.
- vaporization/condensation of Al and Cu; for the sake of simplicity, they are treated similarly to heterogeneous reactions, based on the gas/liquid equilibrium through reactions R4, R6.
- heterogeneous reaction of gaseous Al suboxide species (Al_2O, Al_2O_2, AlO, AlO_2, all referred to as Al_xO_y) on the surface of both Al and CuO particles through reactions R7 to R14. We define the subset of reactions R_{AlxOy} as $R_{AlxOy} = [R7 - R14]$.

The total set of heterogeneous (R1 to R14) and gaseous (R15) reactions is refered as R.

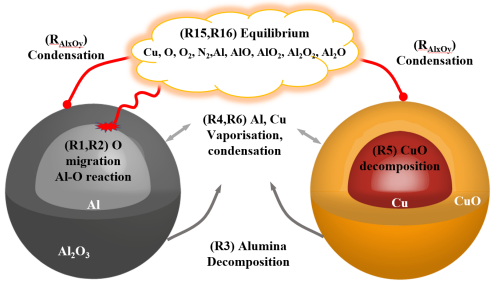

Fig. 1: Schematic view of thermite main reactions occurring on each particle: Al and CuO.

Table 1: List of reactions

Reactions	n°
$2Al_{(c)} + \frac{3}{2}O_{2(g)} \rightarrow Al_2O_{3(c)}$	$R1$
$2Al_{(c)} + 3O_{(g)} \rightarrow Al_2O_{3(c)}$	$R2$
$Al_2O_{3(c)} \rightarrow 2Al_{(g)} + \frac{3}{2}O_{2(g)}$	$R3$
$Al_{(c)} \rightleftharpoons Al_{(g)}$	$R4$
$CuO_{(c)} \rightarrow Cu_{(c)} + \frac{1}{2}O_{2(g)}$	$R5$
$Cu_{(c)} \rightleftharpoons Cu_{(g)}$	$R6$
$Al_2O_{(g)} + O_{2,(g)} \rightarrow Al_2O_{3(c)}$	$R7$
$AlO_{(g)} + \frac{1}{4}O_{2,(g)} \rightarrow \frac{1}{2}Al_2O_{3(c)}$	$R8$
$Al_2O_{2,(g)} + \frac{1}{2}O_{2,(g)} \rightarrow Al_2O_{3(c)}$	$R9$
$AlO_{2,(g)} \rightarrow \frac{1}{4}O_{2,(g)} + \frac{1}{2}Al_2O_{3(c)}$	$R10$
$Al_2O_{(g)} \rightarrow \frac{4}{3}Al_{(g)} + \frac{1}{3}Al_2O_{3(c)}$	$R11$
$AlO_{(g)} \rightarrow \frac{1}{3}Al_{(g)} + \frac{1}{3}Al_2O_{3(c)}$	$R12$
$Al_2O_{2,(g)} \rightarrow \frac{2}{3}Al_{(g)} + \frac{2}{3}Al_2O_{3(c)}$	$R13$
$AlO_{2,(g)} + \frac{1}{3}Al_{(g)} \rightarrow \frac{1}{3}Al_2O_{3(c)}$	$R14$
$\mathrm{Al}_x\mathrm{O}_{y,(g)} \rightleftharpoons x\,\mathrm{Al}_{(g)} + y\,\mathrm{O}_{(g)}$ for $[x,y]\in[0,1,2]^2$	$R15$

R1 to R14 are explicitly treated over time through a system of differential equations. Each reaction r is caracterized by the involved chemical species i and the phase the species belongs to $k = p, q, g$. Gaseous reactions R15 exhibit much faster kinetics than the transport and condensed decomposition mechanisms [13], hence the gas is considered at chemical equilibrium at gas temperature.

2.1. Transfer equations

For condensed phases, the conservation equations of mass and energy are respectively Equation (1) and (2) :

$$N_k \frac{dm_{i,k}}{dt} = \sum_{r\in R} \dot{\omega}^r_{i,k} \tag{1}$$

where N_k is the number of particles in a given phase k ($k = p, q$). $m_{i,k}$ is the mass of the species i in the phase k. $\dot{\omega}^r_{i,k}$ is the reaction rate of the species i from reaction r relative to particle k.

The enthalpy variation for a given particle phase $k = p, q$ is given by Equation (2) :

$$N_k \frac{dH_k}{dt} = \sum_{m\neq k} Q_{m\rightarrow k} + Q_{init} \tag{2}$$

H_k is the enthalpy of one particle of the particle phase k. Considering the particles as isothermal, it is defined as : $H_k = \sum_i m_{i,k} h_i(T_k)$ where $h_i(T_k)$ is the total specific enthalpy of the species i at T_k taking into consideration the formation and sensible enthalpy. $h_i(T_k)$ considers the variation of both the heat capacity and phase change of species i. $Q_{m\rightarrow k}$ is the heat flux received by a given particle phase k from either the other particle phase or the gas. Heat fluxes are symmetric, hence for any condensed or gaseous phase m and k, $Q_{m\rightarrow k}$ equals to $-Q_{k\rightarrow m}$. Q_{init} is the energy flux brought to the Al and CuO particles to initiate the reactions.

For the gas phase, the mass conservation equation is :

$$\frac{d}{dt}(\rho_g \alpha_g V) = \sum_{r\in R}\sum_i \dot{\omega}^r_{i,g} = \Gamma_g \tag{3}$$

where $\dot{\omega}^r_{i,g}$ and Γ_g are the gas production rate of the species i and the total mass flux going from all the particles to the gas, respectively. Due to mass conservation, the global system respects $\sum_{k\in[p,q,g]}\sum_i \dot{\omega}^r_{i,k} = 0$ for each r.

The species conservation equations are defined for each gaseous species i :

$$\frac{d}{dt}(\rho_g \alpha_g V Y_{i,g}) = \sum_{r\in R} \dot{\omega}^r_{i,g} \tag{4}$$

where ρ_g and α_g are the density and volume fraction of the gas phase, respectively. V is the volume of the system, $Y_{i,g}$ is the mass fraction of the species i.

The gas energy conservation equation is :

$$\frac{d}{dt}(\rho_g \alpha_g V u_g) = \sum_{m=p,q} Q_{m\rightarrow g} \tag{5}$$

where $u_g = \sum_i Y_i u_{i,g}(T_g)$ is the specific total intern energy of the gas at T_g. $u_{i,g}(T_g)$ is the specific total intern energy of the gaseous species i at T_g, considering both formation and sensible energy. $Q_{m\rightarrow g}$ represents the energy fluxes received by the gas from the particle phase m.

2.2. Mass exchange and source term modelling

The details of mass variation terms of Equation (1) resulting from the heterogeneous reactions are specified in this section for the particle phases p and q. Reaction times are very small compared to mass transport characteristic times (by diffusion and inter-phase mass fluxes) as reported on previous DFT calculations [14]. Thus, all the reaction rates of heterogeneous reactions (R1 to R14) are supposed limited by mass transport mechanisms and are written as functions of mass fluxes [15].

2.2.1. Al particles (p)

The aluminum oxidation rate $\dot{\omega}^{R1}_{Al,p}$ in the aluminum core is limited by the O_2 transport flux through the boundary layer and the alumina shell. Using a Spalding formulation as detailed in Equation (7) [16], a first mass flux is integrated over the boundary layer, and a second one is integrated over the alumina shell. Assuming a steady state, both fluxes are equal, and an analytical solution of the O_2 mass fraction at the surface of the particle Y^s_{O2} is determined. The O_2 flux $\Phi^{Sp}_{O2,g\to p}$ is computed by injecting Y^s_{O2} in one of the two Spalding formulation. Similar treatment is applied for the oxidation rate relative to the reaction R2.

Thus, the reaction rates of O_2 and O relative to aluminum core oxydation reaction are :

$$\dot{\omega}^r_{i,g} = \Phi^{Sp}_{i,g\to p} \tag{6}$$

for $r = (R1, R2)$ and $i = O_2, O$. Reaction rates of the other species (Al_2O_3 and Al) relative to R1 and R2 are trivially determined using the stoichiometric ratios and molar masses of each species.

The Spalding transport flux in the boundary layer of a species i is defined for $K = 1$, $Y^{out}_i = Y_{i,g}$, $Y^{in}_i = Y^s_i$, $\rho_n = \rho_g$, $D_{i,n} = D_{i,g}$ as :

$$\Phi^{Sp}_{i,g\to p} = -2\pi d_p \rho_n D_{i,n} \log\left(\frac{1 - Y^{out}_i}{1 - Y^{in}_i}\right) K \tag{7}$$

where $D_{i,g}$, Y^s_i are the diffusion coefficients in the gas and the mass fraction at the particle surface of the species i, respectively. For the flux transport in a finite media between d^{in}_p and d_p, the Spalding formulation is defined for $K = d^{in}_p/(d_p - d^{in}_p)$, $Y^{out}_i = Y^s_i$, $Y^{in}_i = 0$ (instantaneous oxidation assumption), $\rho_n = \rho_g$, $D_{i,n} = D_{i,Al2O3}$; where $D_{i,Al2O3}$ is the diffusion coefficient of the species i in the porous alumina shell, which follows an Arrhenius law. Note that as the aluminum is oxidized, the alumina shell grows consequently, increasing the barrier for O_2 and O transport.

$\dot{\omega}^{R4}_{Al,p}$ and $\dot{\omega}^{R6}_{Cu,p}$ correspond to the vaporization/condensation of aluminum and copper respectively, expressed using Equation (7). The surface mass fractions are estimated by their staturated values obtained by a Clapeyron law at the temperature T_p. Since the evaporation is restricted to the surface where the species i is available, the surface ratio defined as $A_{i,p} = (V_{i,p}/\sum_j V_{j,p})^{2/3}$ is introduced; where $V_{i,p}$ is the volume occupied by the species i in the particle p. Thus, the evaporation mass rate is $\dot{\omega}^{R4,R6}_{i=\{Al \atop Cu\},p} = \Phi^{Sp}_{i,g\to p} A_{i,p}$. The condensation mass rate formulation is similar to evaporation but with $A_{i,p} = 1$ as it happens on the whole particle surface.

Reaction rates relative to the set of reactions R_{AlxOy}, result from the heterogeneous reactions of gaseous Al suboxides, on the Al particle surface. Again, surface reactions involving the species i are assumed to be much faster than the diffusion of the species in the gas. Therefore, $Y^s_i = 0$ and the reaction rates relative to R_{AlxOy} are defined by Equation (6) for $r \in [R7 - R14]$ and $i \in Al_xO_y$. By defining the atomic richness of the suboxide gaseous mass fluxes as :

$$\phi_{AlxOy} = \frac{\frac{1}{2}\sum_{i\in AlxOy} \frac{\Phi_{i,g\to p}}{W_i} n^{Al}_i}{\frac{1}{3}\sum_{i\in AlxOy} \frac{\Phi_{i,g\to p}}{W_i} n^{O}_i} \tag{8}$$

where n^{Al}_i and n^O_i are the number of element Al and O in the molecule i respectively, Baijot *et al.* emphasized two possible reactionnal schemes explicited here, composed of $R'_{AlxOy} = [R7, R8, R9, R10]$ when $\phi_{AlxOy} > 1$ and $R''_{AlxOy} = [R11, R12, R13, R14]$ otherwise [6].

The total production rate of Al_2O_3: $\dot{\omega}^{R_{AlxOy}}_{Al2O3,p}$, relative to the set of reactions R_{AlxOy} is trivially determined using the stoichiometric ratios and molar masses of each species.

$\dot{\omega}^{R3}_{Al2O3,p}$ is the Al_2O_3 decomposition rate approximated with an Arrhenius law (see Table 2).

2.2.2. CuO particles (q)

CuO particles are composed of CuO, Cu, and possibly recondensed Al or Al_2O_3. Hence, Equation (1) is developped for CuO, Cu, Al and Al_2O_3.

$\dot{\omega}^{R3}_{Al2O3,q}$ and $\dot{\omega}^{R5}_{CuO,q}$ represent the CuO and Al_2O_3 decomposition (reactions R3 and R5), which kinetics are approximated again with an Arrhenius law (see Table 2). The condensed Cu production rate $\dot{\omega}^{R5}_{Cu,q}$ relative to CuO decomposition is trivially determined using the stoichiometric ratios and molar masses of each species.

$\dot{\omega}^{R6}_{Cu,q}$, $\dot{\omega}^{R4}_{Al,q}$ and $\dot{\omega}^{R_{AlxOy}}_{Al2O3,q}$ correspond to the vaporization-condensation of Cu and Al species and the heterogeneous reactions, respectively. These terms are determined similarly to the aluminum particles (see definitions of $\dot{\omega}^{R6}_{Cu,p}$, $\dot{\omega}^{R4}_{Al,p}$ and $\dot{\omega}^{R_{AlxOy}}_{Al2O3,p}$).

2.2.3. Gas phase (g)

For each gaseous species i, Equation (4) is solved in its non conservative form. For all heterogeneous reactions R1 to R14, the production rate of a gaseous species i involved in reaction r may be written in terms of the corresponding reaction rates in the condesed phases, as :

$$\dot{\omega}^r_{i,g} = \sum_{k=p,q} \frac{W_i}{W_j}\frac{\nu^r_i}{\nu^r_j}\dot{\omega}^r_{j,k} = \sum_{k=p,q} \dot{\omega}^r_{i,g(k)} \tag{9}$$

where j is any condensed species of the reaction r (whose reaction rates have been defined previously). $\dot{\omega}^r_{i,g(k)}$ is introduced as the gaseous source term of the species i relative to reaction r taking place on the condensed phase k. ν^r_i is the global molar stoichiometric coefficient of reaction r such as $\nu^r_i > 0$ if i is a product and $\nu^r_i < 0$ otherwise.

Regarding the mass conservation, Equation (3) becomes :

$$\alpha_g V \frac{d\rho_g}{dt} = \left[\Gamma_g - \rho_g V \frac{d\alpha_g}{dt} \right] \quad (10)$$

The gas volume fraction time derivative $\frac{d\alpha_g}{dt}$ is implicitely computed using the relations $\alpha_k = \sum_i N_k m_{i,k} (V \rho_{i,k})^{-1}$ for $k = p, q$ and $\alpha_g = 1 - \sum_{k=p,q} \alpha_k$ where $\rho_{i,k}$ is the condensed density of the species i (assumed constant) and α_k is the volume fraction of the particle phase $k = p, q$.

Finally, all the gaseous reactions rates of R15 and **??** are taken into account by the chemical equilibrium of the gas.

2.3. Heat flux and source terms

The total flux of energy received by a phase $k = p, q, g$, can be generally expressed for any phase m and k as :

$$\sum_{m \neq k} Q_{m \to k} = \sum_{m \neq k} (Q^{cond}_{m \to k} + Q^{rad}_{m \to k} + Q^{species}_{m \to k}) \quad (11)$$

$Q^{species}_{p \to q}$, coupled to the direct mass transfer by contact between both particle phases is not considered. The total particle phase surface is considered much larger than the system boundaries, thus radiation and conduction transfer with walls are neglected.

The conduction between the two particles is written as :

$$Q^{cond}_{p \to q} = H^{cond}_{p \to q} (T_p - T_q) \quad (12)$$

where $H^{cond}_{p \to q}$ is computed based on the particle and intersticial gas conductance and the particle interphase coordination number [17, 18]. Note that only effective contact is considered and the mean coordination number N_{pq} is approximated to 3.

For particle to particle radiative transfer, as the condensed phase surfaces are assumed much larger than the system boundaries, the system can be treated as an enclosed problem [19], then :

$$Q^{rad}_{p \to q} = \frac{\sigma (T_p^4 - T_q^4)}{\frac{1-\varepsilon_p}{A_p \varepsilon_p} + \frac{1}{A_p F_{p \to q}} + \frac{1-\varepsilon_q}{A_q \varepsilon_q}} \quad (13)$$

where $A_k = N_k \pi d_k^2$, and ε_k are the total surface and the emissivity, approximated to 0.85, of the condensed phase k, respectively. Assuming the condensed phases being homogeneously dispersed in the considered volume, the view angle $F_{p \to q}$ is defined as :

$$F_{p \to q} = \frac{N_q d_q^2}{N_q d_q^2 + N_p d_p^2} \quad (14)$$

Second, let's define the energy fluxes from the particle phases $m = p, q$ to the gas phase $k = g$. Radiation between the gas and the particles is assumed negligible leading to consider only the conduction and mass transfer related terms. As no mean relative motion between the gas and the particles is considered for both particle phases, it is defined as:

$$Q^{cond}_{m \to g} = \lambda_g \pi d_m Nu (T_m - T_g) N_p \quad (15)$$

Where λ_g is the gas mixture conductivity and Nu the Nusselt number, equals to $(7 - 10\ \alpha_g + 5\alpha_g^2)$ as stated by Gunn [20]. T_m and T_g are the temperatures of the particle phase m and of the gas g, respectively.

The heat flux related to the mass transfer from the particle phase $m = p, q$ to the gas g is evaluated at the temperature of the phase T^r_σ (for each reaction r), from which the mass flux comes from :

$$Q^{species}_{m \to g} = \sum_{r \neq R15} \sum_i C^r_i \dot{\omega}^r_{i,\sigma} u_{i,(\sigma)} (T^r_\sigma) \quad (16)$$

However, for reactions R1, R2, R4, R5, R6, the difference of formation energy between gaseous and condensed species i is withdrawn from the particle (thus, for example, cooling down the particle during an evaporation process), hence :

$$C^r_i \dot{\omega}^r_{i,\sigma} u_{i,(\sigma)} (T^r_\sigma) = \dot{\omega}^r_{i,g(m)} u_{i,(g)} (T_m) \mathcal{H}(\dot{\omega}^r_{i,g(m)}) - \dot{\omega}^r_{i,g(m)} u_{i,(g)} (T_g) \mathcal{H}(-\dot{\omega}^r_{i,g(m)}) \quad (17)$$

while, for reactions R3 and R_{AlxOy} the difference of formation energy between gaseous and condensed species i is withdrawn from the gas, hence :

$$C^r_i \dot{\omega}^r_{i,\sigma} u_{i,(\sigma)} (T^r_\sigma) = -\dot{\omega}^r_{i,m} u_{i,(m)} (T_m) \mathcal{H}(-\dot{\omega}^r_{i,m}) + \dot{\omega}^r_{i,m} u_{i,(m)} (T_g) \mathcal{H}(\dot{\omega}^r_{i,m}) \quad (18)$$

where $u_{i,(g)}$ and $u_{i,(m)}$ are the total energy of the gaseous and condensed species i, respectively. $\mathcal{H}$ is the heaviside function, specifying that the transfered energy is taken from the phase from which the mass flux of the reaction r comes from.

3. Simulation details and model parameters

The numerical resolution is splitted into two steps:

1. The mass and energy equations for particle phases are integrated over a time step based on the heat flux terms and heterogeneous reaction rates of R1 to R14 using an explicit Euler scheme. Based on the newly computed particle composition, the particle diameters d_p^{n+1} and the gas volume fraction α_g^{n+1} are updated at the iteration $n + 1$. Gaseous intermediate species mass fraction $\tilde{Y}_{i,g}^{n+1}$ and energy $\tilde{u}_g^{n+1}$ are estimated by integrating only the heterogeneous reactions rates and the heat flux terms. A semi-implicit scheme specified by Equation (19), with $\zeta = 1, Y_{i,g}, u_g$ and $\phi_\zeta = \frac{d}{dt}(\rho_g V_g \zeta)$ is used.
2. Based on those intermediate values, the chemical equilibrium is computed at constant energy and density by Cantera [21], leading to the actual species mass fractions and temperature: $Y_{i,g}^{n+1}$, T_g^{n+1} of the gas.

A dynamical computation of the time step is established based on realisability and stability conditions : Δt ranging between 10^{-7} and 10^{-9} s, mainly limited by a user defined maximum gas temperature variation (stability condition) between two iterations.

$$\zeta^{n+1} = \frac{(\rho V_g \zeta)^n + \phi_\zeta^n \Delta t}{(\rho V_g)^n + \Gamma^n \Delta t} \tag{19}$$

3.1. Thermophysical and reaction parameters

All thermodynamical data, for condensed and gaseous species, come from JANAF tables [22]. The gas transport properties are computed based on the Lennard-Jones potential using Cantera [21] considering parameters found in the litterature [23–25]. The vaporization points of the aluminum metal and copper metal evolves with respect to the pressure as a function of a Clapeyron law. The three (k_0, E_a) couples characterizing the kinetic of CuO, Al_2O_3 decomposition and O_x diffusion via an Arrhenius law, were obtained by fitting the theoretical pressure as predicted by the model to already published experimental data [26]. A theoritical study of the kinetic parameters have been performed (not detailed in this article), which results are presented in Table 2.

Table 2: Kinetic parameters

Parameters (units)	Value
$k_0^{R1,R2}$ ($m^2.s^{-1}$)	1.5×10^{-5}
k_0^{R3} ($kg.m^{-3}.s^{-1}$)	1.52×10^{6}
k_0^{R5} ($kg.m^{-3}.s^{-1}$)	2.86×10^{7}
$E_a^{R1,R2}$ ($J.mol^{-1}.K^{-1}$)	75×10^{3}
E_a^{R3} ($J.mol^{-1}.K^{-1}$)	400×10^{3}
E_a^{R5} ($J.mol^{-1}.K^{-1}$)	46×10^{3}

3.2. Initial conditions

The calculations were carried out with the initial temperature of the thermite system being set to 300 K, and adiabatic boundary conditions. The initial characteristics of the gas are calculated at atmospheric conditions. An energy of 600 $kJ.kg^{-1}$ is injected at a power of 2 GW to the set of Al and CuO particles to ignite the system.

4. Results

Two systems of 0.5 g of Al particles, and 1.25 g of CuO particles were simulated and pressure development compared: a nanothermite ($d_p = d_q = 100$ nm) and a microthermite ($d_p = d_q = 5$ µm). Al particle purity, compaction rate and richness of both thermites are set to 0.7, 50 $\%TMD$ and 1.2, respectively. The chamber volume is fixed at 1 cm^3.

Graphs (a,c,e,g) and (b,d,f,h) of Fig. 2 show the temporal evolution of the main observables of nano and microthermite respectively. The self-sustained combustion starts when Al particles reach 1162 K and 1133 K after 0.75 µs and 0.9 µs for nano and microthermite respectively. Both systems converge to the same equilibrium state at the end of the reaction, with a temperature of 4300 K and a pressure of 22 MPa. Particle outer diameters change only slightly as

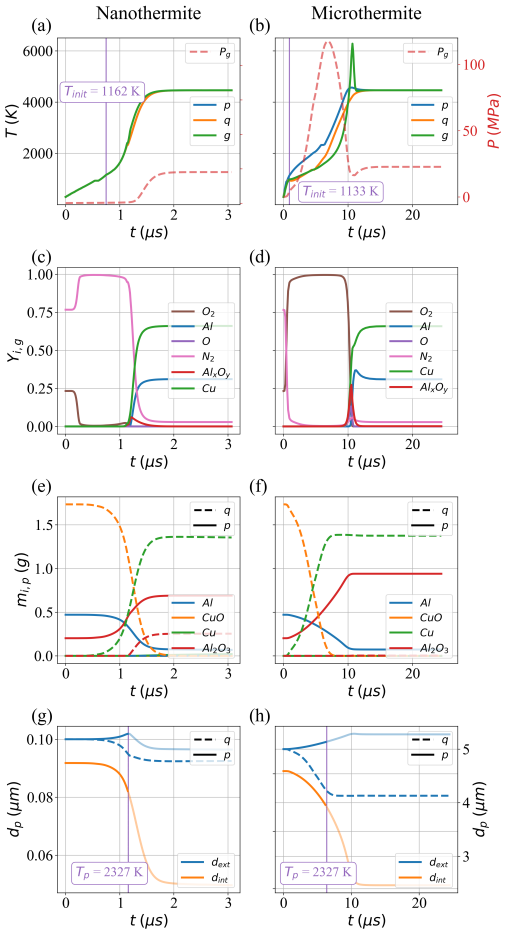

Fig. 2: Time evolution for a nanothermite (a,c,e,g) and microthermite system (b,d,f,h) of : (a,b) the temperature of each phase (solid line) and gas pressure (dashed line), (b,d) the mass fraction of each species in the gas, (e,f) the species condensed mass in the system, (g,h) the Al particle inner (orange) and outer (blue) diameters and the for CuO particle outer diameter (dashed blue) $d_p = d_q = 100$ nm and 5 µm

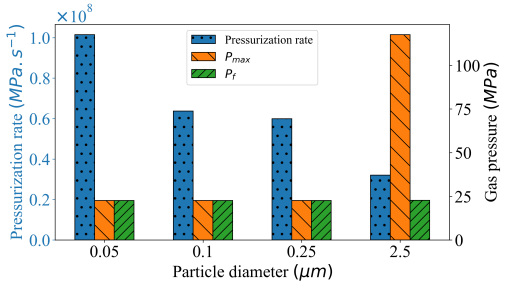

Fig. 3: Pressurization rate, maximum and final gas pressure with respect to particle initial diameters $d_p = d_q$

condensed Al and CuO are replaced by Al_2O_3 and Cu.

Nanothermite features a delayed pressurization compared to the temperature rise (Fig. 2a), which indicates that a first combustion regime (from 0.75 to 1.2 µs) occurs in the condensed phase. In that regime, all the released O_2 by the CuO decomposition is captured by the large Al particles specific area (11.89 $m^2.g^{-1}$). After diffusion through the shell and reaction with the Al core, oxygen absorption leads to the Al_2O_3 growth. In the meantime, condensed Cu is generated through the CuO decomposition in the CuO particle phase (Fig. 2e). The alumina shell, characterized by the difference between the inner and outer diameters (see Fig. 2g orange and blue lines, respectively) increases during the condensed combustion process, thus increasing the resistance of Al_2O_3 barrier to Al oxydation. The purple vertical lines (on Fig. 2g,h) represent the moment when the temperature of the Al particle reaches the temperature of alumina liquefaction at 1.2 µs. At that point, the model of alumina shell may become questionnable. Right after reaching the alumina liquefaction temperature, the diameter of Al particle p starts deacreasing, as liquid Al evaporates, decreasing the amount of matter in the particle. The vaporized Al partially reacts with O_x in the gas to produce Al_xO_y (mainly Al_2O), as shown from the evolution of the gas temperature being above the temperature of the particle phases. These suboxides then react quasi-instantaneously onto the CuO particles to generate Al_2O_3 (Fig. 2e). This fast kinetic scheme is supported by the fact that the Al_xO_y mass fractions are very low in the gas phase (Fig. 2c). Meanwhile alumina becomes liquid at 1.2 µs and temperature is higher than 2300 K, Al and Cu species start to vaporize (Fig. 2c) into the gas leading to a pressure rize (Fig. 2a). The pressure reaches a maximum when CuO is totally reduced (Fig. 2e) at 4300 K. An equilibrium state is thus obtained at $\sim$1.8 µs. During the whole simulated time, the three phases are almost at the same temperature (Fig. 2a), heat fluxes being very efficient due to the large specific are in nanothermite system. To sum up, two very clear combustion regimes are observed :

- A first condensed combustion regime when the oxygen coming from the CuO decomposition is absorbed by the Al particle, reacting with the Al in the core, until the temperature of liquefaction of alumina is reached at 1.2 µs.
- A second regime, where the gas drives the reactions through the species and energy transport between both particle phases.

By contrast, in the microthermite system, the specific area being very small (0.23 $m^2.g^{-1}$) the O_2 absorption on the Al particles surface is limited leading to a slight increase of alumina shell (Fig. 2h). Indeed, in microthermite, volume reactions are much faster than the surface ones. Therefore, the Al particles do not have the time to absorb all the oxygen coming from the CuO decomposition. Hence, the gas becomes an intermediate tank for O_2, damping the characteristic time differences between the surface and volume mechanisms, as the pressure rises up to 115 MPa at 7 µs.

When the pressure starts decreasing (Fig. 2b) due to oxygen absorption on the aluminum particles, Al evaporation is finally enabled at 10 µs, increasing drastically the gas temperature up to 6000 K because of the reaction with gaseous oxygen. Al_xO_y, mainly consisting of AlO, do not react on the particle surface as fast as in the nanothermite system and their mass fraction reach 0.25 (Fig. 2d). When the Al_xO_y species recondense, the system converges to its equilibrium state at 12 µs. Contrary to the nanothermite system, the three phases are at relatively different temperature (Fig. 2b). This is explained by the fact that the heat fluxes are less efficient due to the smaller specific area. Note also that, compared to nanothermite, Al_2O_3 produced on CuO particles is negligible (Fig. 2f).

This behavior corroborates the experimental measurements by Nicollet *et al.* [27] showing an overpressure peak prior to the establishment of a lower final pressure in Al/CuO nanothermites. Nevertheless, simulated pressurization rates are at least one order of magnitude higher than the ones observed experimentally, which can be explained by an insufficiently accurate estimation of the kinetic parameters (k_0, E_a in Table 2) or by an overestimation of the particle surfaces that can actually agglomerate through reactive sintering.

Finally, Fig. 3 confirms the great impact of the Al particle size on the pressure development in the bomb chamber. The maximum pressurization rate increases with decreasing Al particles size as often characterized experimentally [28]. As discussed previsouly, the nanothermite system features a maximum pressure (P_{max}) due to Cu and Al gaseous species, equal to the final pressure (P_f) as no heat losses are considered here, whereas microthermite develops a pressure peak at low temperature $P_{max} = 115$ MPa related to gaseous oxygen, before stabilizing at 22 MPa through gaseous Cu and Al.

5. Conclusion

A 0D Al/CuO thermite combustion model has been developped taking into consideration the different mechanisms identified in a Al/CuO reaction in a closed volume, which shows the same temporal behavior and a final pressure in the same order of magnitude as experimental data ($\sim$ 20 MPa) [26]. This model enables, for the first time, a closer examination of kinetical mechanisms driving thermite combustion. Different combustion regimes were observed depending on the particle size. They are explained by the difference in specific area between the two simulated thermite systems (11.89 $m^2.g^{-1}$ vs. 0.23 $m^2.g^{-1}$).

In addition, this theoritical tool can be used to predict closed-bomb experiment and can serve as a foundation for a multi-dimensionnal propagating model.

Acknowledgement

The authors acknowledge support from the European Research Council (H2020 Excellent Science) Researcher Award (grant 832889 – PyroSafe) and ArianeGroup which funds Emelian Tichtchenko scholarship.

References

[1] K. Kim, Computational modeling of combustion wave in nanoscale thermite reaction, International Journal of Energy and Power Engineering 8 (7) (2014) 679–682.

[2] S. Brotman, M. Djafari Rouhani, S. Charlot, A. Estève, C. Rossi, A Benchmark Study of Burning Rate of Selected Thermites through an Original Gasless Theoretical Model, Applied Sciences 11 (14) (2021) 6553.

[3] N. W. Piekiel, L. Zhou, K. T. Sullivan, S. Chowdhury, G. C. Egan, M. R. Zachariah, Initiation and Reaction in Al/Bi $_2$ O $_3$ Nanothermites: Evidence for the Predominance of Condensed Phase Chemistry, Combustion Science and Technology 186 (9) (2014) 1209–1224.

[4] E. Tichtchenko, A. Estève, C. Rossi, Modeling the self-propagation reaction in heterogeneous and dense media: Application to al/cuo thermite, Combustion and Flame 228 (2021) 173–183.

[5] J. M. Epps, J.-P. Hickey, J. Z. Wen, Modelling reaction propagation for Al/CuO nanothermite pellet combustion, Combustion and Flame 229 (2021) 111374.

[6] V. Baijot, D.-R. Mehdi, C. Rossi, A. Estève, A multiphase micro-kinetic model for simulating aluminum based thermite reactions, Combustion and Flame 180 (2017) 10–19.

[7] C. Lanthony, J.-M. Ducéré, A. Estève, C. Rossi, M. Djafari-Rouhani, Formation of Al/CuO bilayer films: Basic mechanisms through density functional theory calculations, Thin Solid Films 520 (14) (2012) 4768–4771.

[8] G. Xiong, C. Yang, W. Zhu, Interface reaction processes and reactive properties of Al/CuO nanothermite: An ab initio molecular dynamics simulation, Applied Surface Science 459 (2018) 835–844, publisher: Elsevier.

[9] A. Rai, K. Park, L. Zhou, M. R. Zachariah, Understanding the mechanism of aluminium nanoparticle oxidation, Combustion Theory and Modelling 10 (5) (2006) 843–859.

[10] H. Nie, M. Schoenitz, E. L. Dreizin, Initial stages of oxidation of aluminum powder in oxygen, Journal of Thermal Analysis and Calorimetry 125 (1) (2016) 129–141, publisher: Springer.

[11] M. Mursalat, C. Huang, B. Julien, M. Schoenitz, A. Esteve, C. Rossi, E. L. Dreizin, Low-Temperature Exothermic Reactions in Al/CuO Nanothermites Producing Copper Nanodots and Accelerating Combustion, ACS Applied Nano Materials 4 (4) (2021) 3811–3820.

[12] C. Lanthony, M. Guiltat, J. M. Ducéré, A. Verdier, A. Hémeryck, M. Djafari-Rouhani, C. Rossi, Y. J. Chabal, A. Estève, Elementary surface chemistry during CuO/Al nanolaminate-thermite synthesis: copper and oxygen deposition on aluminum (111) surfaces, ACS applied materials & interfaces 6 (17) (2014) 15086–15097, publisher: ACS Publications.

[13] J. Suarez, Modélisation de la combustion diphasique de l'aluminium et application sur la post-combustion d'une charge explosive condensée dans l'air, Ph.D. thesis (2020).

[14] C. Lanthony, J. M. Ducéré, M. D. Rouhani, A. Hemeryck, A. Estève, C. Rossi, On the early stage of aluminum oxidation: An extraction mechanism via oxygen cooperation, The Journal of Chemical Physics 137 (9) (2012) 094707.

[15] I. Glassman, R. A. Yetter, N. G. Glumac, Combustion, Academic press, 2014.

[16] K. K. Kuo, Principles of combustion (1986).

[17] G. K. Batchelor, R. O'brien, Thermal or electrical conduction through a granular material, Proceedings of the Royal Society of London. A. Mathematical and Physical Sciences 355 (1682) (1977) 313–333.

[18] M. Moscardini, Y. Gan, S. Pupeschi, M. Kamlah, Discrete element method for effective thermal conductivity of packed pebbles accounting for the smoluchowski effect, Fusion Engineering and Design 127 (2018) 192–201.

[19] M. N. Ozisik, Heat transfer: a basic approach, Vol. 1, McGraw-Hill New York, 1985.

[20] D. Gunn, Transfer of heat or mass to particles in fixed and fluidised beds, International Journal of Heat and Mass Transfer 21 (4) (1978) 467–476.

[21] D. G. Goodwin, R. L. Speth, H. K. Moffat, B. W. Weber, Cantera: An Object-oriented Software Toolkit for Chemical Kinetics, Thermodynamics, and Transport ProcessesVersion 2.5.1 (2021).

[22] J. Malcolm W. Chase, NIST-JANAF thermochemical tables, Fourth edition. Washington, DC : American Chemical Society ; New York : American Institute of Physics for the National Institute of Standards and Technology, 1998., 1998.

[23] R. A. Svehla, Estimated viscosities and thermal conductivities of gases at high temperatures, Vol. 132, National Aeronautics and Space Administration, 1963.

[24] O. Orlandi, Modélisation et simulation n umérique de la combustion d'une goutte isolée d'aluminiumPublisher: Orléans (2002).

[25] V. Filippova, S. Kunavin, M. Pugachev, Calculation of the parameters of the lennard-jones potential for pairs of identical atoms based on the properties of solid substances, Inorganic Materials: Applied Research 6 (1) (2015) 1–4.

[26] L. Glavier, G. Taton, J.-M. Ducere, V. Baijot, S. Pinon, T. Calais, A. Esteve, M. D. Rouhani, C. Rossi, Nanoenergetics as pressure generator for nontoxic impact primers: comparison of al/bi2o3, al/cuo, al/moo3 nanothermites and al/ptfe, Combustion and Flame 162 (5) (2015) 1813–1820.

[27] A. Nicollet, L. Salvagnac, V. Baijot, A. Estève, C. Rossi, Fast circuit breaker based on integration of Al/CuO nanothermites, Sensors and Actuators A: Physical 273 (2018) 249–255.

[28] M. Weismiller, J. Malchi, J. Lee, R. Yetter, T. Foley, Effects of fuel and oxidizer particle dimensions on the propagation of aluminum containing thermites, Proceedings of the Combustion Institute 33 (2) (2011) 1989–1996.